AGU100 ADVANCING EARTH AND SPACE SCIENCE

Geophysical Research Letters

RESEARCH LETTER

10.1029/2018GL081658

Key Points:

- We cross-correlate Birkeland current density with IMF B_y and B_z and find morphology of R1/R2 and other current systems
- B_z direct driving timescales are 10-20 min; expanded polar cap timescales, 60-90 min; and nightside timescales, 120-150 min
- B_y shows 10-min timescales on the dayside at high latitudes, but lags up to 240 min elsewhere

Supporting Information:

- Supporting Information S1
- Supporting Information S2
- Figure S1
- Figure S2

Correspondence to:
J. C. Coxon,
work@johncoxon.co.uk

Citation:
Coxon, J. C., Shore, R. M., Freeman, M. P., Fear, R. C., Browett, S. D., Smith, A. W., et al. (2019). Timescales of Birkeland currents driven by the IMF. *Geophysical Research Letters*, *46*. https://doi.org/10.1029/2018GL081658

Received 17 DEC 2018
Accepted 21 FEB 2019

Timescales of Birkeland Currents Driven by the IMF

John C. Coxon[1], Robert M. Shore[2], Mervyn P. Freeman[2], Robert C. Fear[1], Stephen D. Browett[1], Andrew W. Smith[1], Daniel K. Whiter[1], and Brian J. Anderson[3]

[1]School of Physics and Astronomy, University of Southampton, Southampton, UK, [2]British Antarctic Survey, Cambridge, UK, [3]The Johns Hopkins University Applied Physics Laboratory, Laurel, MD, USA

Abstract We obtain current densities from the Active Magnetosphere and Planetary Electrodynamics Response Experiment (AMPERE), alongside B_y and B_z from the Interplanetary Magnetic Field (IMF) for March 2010. For each AMPERE spatial coordinate, we cross-correlate current density with B_y and B_z, finding the maximum correlation for lags up to 360 min. The patterns of maximum correlation contain large-scale structures consistent with the literature. For the correlation with B_y, the lags on the dayside are 10 min at high latitudes but up to 240 min at lower latitudes. Lags on the nightside are 90–150 min. For B_z, the shortest lags on the dayside are 10–20 min; on the equatorward edge of the current oval, 60–90 min; and on the nightside, predominantly 90–150 min. This novel approach enables us to see statistically the timescales on which information is electrodynamically communicated to the ionosphere after magnetic field lines reconnect on the dayside and nightside.

Plain Language Summary We take the minute-by-minute behavior of the interplanetary magnetic field (which is in the solar wind) and electric currents flowing along Earth's magnetic field lines in the Northern Hemisphere. We move them with respect to one another to find the time lag required to make them agree best, and then note the best agreement and the time lag that we found. We plot both of these quantities on maps of the Earth's Northern Hemisphere, and then analyze these maps to uncover new information about Earth's reaction to the solar wind.

1. Introduction

Birkeland currents (also known as field-aligned currents) were first observed by Zmuda et al. (1966) as magnetic perturbations, which Cummings and Dessler (1967) later recognized as the current systems of Birkeland (1908, 1913), hence their name. The statistical pattern of the currents was outlined a decade after their discovery (Iijima & Potemra, 1978), revealing two regions of Birkeland current: Region 1 (R1) has been shown to be colocated with the open/closed field-line boundary (Clausen et al., 2013), and Region 2 (R2) is a region equatorward of this (therefore, on closed field lines). Examination of the statistical patterns of the currents with clock angle show that Birkeland current density is enhanced when the interplanetary magnetic field (IMF) is southward (e.g., Weimer, 2001), and it has also been established that Birkeland currents are enhanced when the dayside or nightside reconnection rates are higher (Coxon et al., 2014a, 2014b; Coxon et al., 2016, 2017). Birkeland currents are the mechanism by which stress is transmitted from the magnetosphere to the ionosphere, and as such, they tell us about how processes such as reconnection at the magnetopause and in the magnetotail affect the ionosphere (e.g., Cowley, 2000; Southwood & Hughes, 1983).

Previous studies have looked at the timescales on which currents react to IMF driving. Anderson et al. (2014) lagged Advanced Composition Explorer (ACE) data to Earth (to 0 R_E in geocentric coordinates) and then presented case studies in which the Regions 1 and 2 current systems on the dayside appeared within 20 min of B_z turning southward, with nightside currents appearing 60–90 min after the southward turning. Currents at dawn and dusk intensified after that, yielding a fully formed R1 and R2 system 120 min after the turning in B_z. Anderson et al. (2017) also examined the evolution of Birkeland currents during a geomagnetic storm, but the focus of that paper was comparing Active Magnetosphere and Planetary Electrodynamics Response Experiment (AMPERE) data to modeled results. Anderson et al. (2014) interpreted their findings as evidence that the formation of the current systems was associated with the onset of flows in the ionosphere which evolve on similar timescales. The timescale for this is bimodal. Following the onset of reconnection at the

magnetopause, flows respond within minutes near noon and progressively later at later local times (e.g., Freeman, 2003, and references therein). Later, after an hour or so, flows are again (analogously) excited by the onset of nightside reconnection (Cowley & Lockwood, 1992).

Asymmetries in dayside convection and currents are also introduced by the IMF B_y component due to longitudinal stresses on newly reconnected field lines at the magnetopause (Greenwald et al., 1990; Saunders, 1989). As with the response to IMF B_z associated with magnetopause reconnection, the response to IMF B_y is within minutes near noon and later toward dawn and dusk (Saunders et al., 1992). It has long been thought that these B_y asymmetries propagate into the magnetotail via convecting field lines (Cowley, 1981), and so it can be reasonably supposed that the subsequent reconnection of these asymmetric field lines in the tail will create flow and current asymmetries with timescales similar to the nightside B_z case. The timescales of the Dungey (1961) cycle and the expanding/contracting polar cap (ECPC) paradigm (Cowley & Lockwood, 1992; Siscoe & Huang, 1985) suggest that field lines should take of the order of hours to convect from the dayside into the magnetotail. Browett et al. (2017) showed that the timescales of propagation of B_y components from the IMF into the magnetotail are bimodal, and have a timescale of ∼1 hr for southward B_z and ∼3 hr for northward B_z, consistent with work on magnetospheric dynamics during northward IMF (Fear & Milan, 2012). Time History of Events and Macroscale Interactions during Substorms (THEMIS) observations from throughout the magnetotail have been used to examine the propagation of the B_y asymmetry in the tail, and show that this asymmetry propagates into the inner magnetosphere from downtail (Pitkänen et al., 2016), also consistent with the idea that asymmetries propagate due to convecting field lines.

Information can propagate into the magnetosphere more quickly than field line convection via Alfvén waves. It has been suggested that these waves can cause the Birkeland currents to react almost instantaneously to increases in dayside reconnection (Snekvik et al., 2017) and induce a B_y asymmetry in the magnetotail in the same sense as the IMF on timescales of 15–45 min (Khurana et al., 1996; Tenfjord et al., 2015), and it has been shown that this mechanism can induce asymmetries on closed field lines (Tenfjord et al., 2017, 2018).

2. AMPERE and OMNI

In this paper, data from AMPERE are employed. This data set uses spherical harmonics and Ampere's law to take magnetic perturbations measured in situ by the Iridium telecommunications satellite network and calculate vertical current densities j (Anderson et al., 2000, 2014; Waters et al., 2001), which are available at a resolution of 1° colatitude and 1 hr of MLT in altitude-adjusted corrected geomagnetic (AACGM) coordinates. We note that using AMPERE data to investigate Birkeland currents assumes that the field lines are vertical, and the spherical harmonic process may introduce some smoothing of the correlations and lags reported in this paper. In terms of cadence, the data are evaluated in a sliding window 10 min long, which is evaluated every 2 min: we note that this will affect the accuracy of the timelags found in this paper. When comparing AMPERE data with IMF data, we adopt the timestamp of the middle of the sliding window, as opposed to Anderson et al. (2014), who used the end of the sliding window. We adopt the common convention, when using AMPERE data, that upward currents have positive j and downward currents have negative j. A review of the work that has been done with AMPERE is presented in Coxon et al. (2018).

This paper also employs OMNI data (King & Papitashvili, 2014), which presents data from a variety of spacecraft, lagged to the bow shock. We utilize the B_y and B_z components of the IMF in geocentric solar magnetospheric coordinates in this study.

Lastly, within this paper we use a cross-correlation technique inspired by the Spatial Information from Distributed Exogenous Regression (SPIDER) technique developed and applied to SuperMAG data by Shore et al. (2019). We do a Pearson cross-correlation of the time series of B_z and B_y during the month of March 2010 with the current density observed by the AMPERE data set j at each spatial coordinate and for time lags varying from 0–6 hr. We note that we do not compute time lags lower than 0 hr, such that we do not allow the behavior of the Birkeland currents to precede that of the IMF. We plot the best correlation coefficients for both components of the IMF in Figures 1a and 2a with the same coordinates as the constituent AMPERE data. For correlations under 0.1 we fill the coordinate in white in both maps. We emphasize that each correlation in this paper is computed between time series which comprise the entirety of March 2010, varied by 0–6 hr, such that each correlation is between time series which are ∼31 days long. The cross-correlation functions for each coordinate in Figures 1 and 2 are presented in the supporting information.

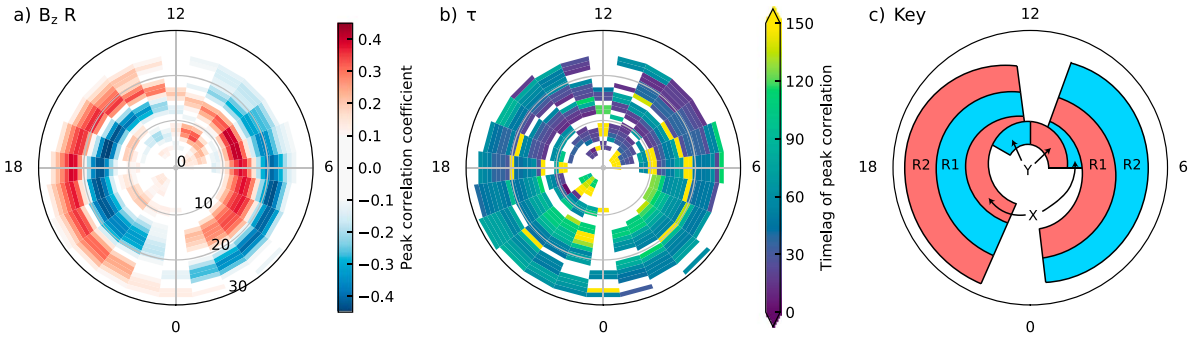

Figure 1. (a) The maximum correlation of B_z with j. (b) The lag at which the maximum correlation was achieved. (c) Key to aid interpretation of the left two panels. White cells indicate coordinates for which the maximum correlation was under 0.1. Note that the color bar on the left is not saturated, whereas the color bar in the center is saturated at 150 min.

3. Cross-Correlation of IMF Components With Birkeland Current Density j

Figure 1a shows that the regions of maximum correlation with the IMF B_z lie on two concentric rings of about 13° and 21° radius centered a few degrees antisunward of the geomagnetic pole. Each of the correlations in Figure 1a lies more than 2σ from the mean correlation in that coordinate. The locations of these regions are clearly identified with the Regions 1 and 2 Birkeland current (Iijima & Potemra, 1978), which may be understood because negative B_z mostly drives these Birkeland currents. Therefore, positive correlations are associated with downward Birkeland current and vice versa. We will describe the regions of correlation associated with the R1 and R2 current as the R1 correlation and the R2 correlation for the convenience of the reader. The R1 and R2 correlations are not as well defined in the midnight MLT sector, and the positive correlation looks like a spiral, as the positive R1 and R2 correlations are linked at noon MLT: These features are very reminiscent of the statistical patterns reported by Iijima and Potemra (1978). In addition to the R1 and R2 correlations, there are regions of correlation which are of the opposite sense to the R1 correlation and ~2° poleward, which we refer to as the X correlations. There are also more localized and slightly weaker regions of correlation in the dayside polar cap which are the same sense as the R1 correlations but which are displaced ~5° poleward of the R1 correlation: we refer to these as the Y correlations. All four of

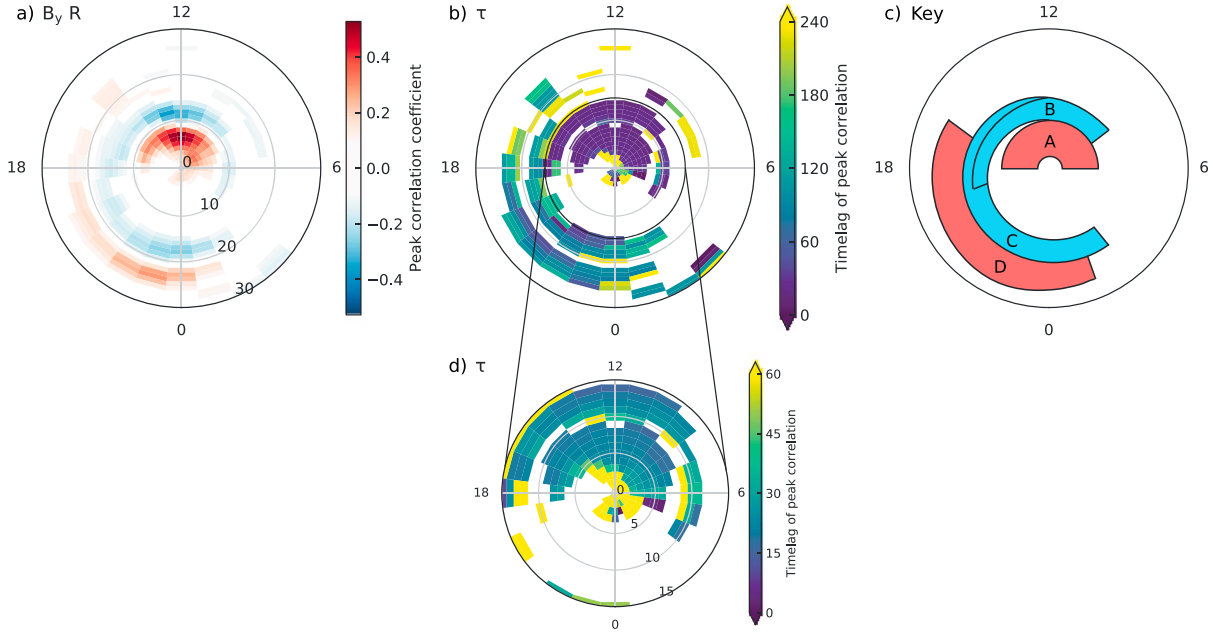

Figure 2. (a) The maximum correlation of B_y with j. (b) The lag at which the maximum correlation was achieved, saturated at 240 min. (c) Key to aid interpretation of the left two panels. (d) A zoomed-in view of part of the center panel, saturated at 60 min. White cells indicate coordinates for which the maximum correlation was under 0.1.

these are indicated on the key in Figure 1c. We note here that, unlike the R1 and R2 correlations, our choice of terminology for the X and Y correlations is solely intended to refer to the spatial regions indicated—that is, we do not intend to imply any causation with external variables. We will discuss the potential cause of the X and Y correlations later in the paper.

Similarly, the maximum correlation between B_y and j is presented in Figure 2a, in the same format as Figure 1a. Each of the correlations in Figure 2a lies more than 2σ from the mean correlation in that coordinate. There are two regions of correlation centered on noon MLT: a positive correlation located within a colatitude of 10°, which we denote the A correlation; and a negative correlation located between 10°–15°, the B correlation. Both of these correlations are limited solely to the dayside. A region of negative correlation starts at approximately 16 MLT and extends to 2 MLT just poleward of 20° colatitude: this is the C correlation. The region of positive correlation which is equatorward of and extends 1 hr less than the C correlation in each direction is the D correlation. Figure 2c shows the locations of these correlations. The labels for these correlations are, again, solely intended to refer to the spatial regions indicated and are not intended to imply causation with external variables.

4. The Timescales of the Identified Regions of Correlation

The timescales of the identified correlation regions are shown in Figures 1b and 2b. In both cases, the cross-correlation was performed up to time lags of 6 hr. For each coordinate contributing to the maps in Figures 1a and 2a we plot the correlation coefficient against the time lag in order to see how the lag affects the correlation. These plots of the correlation coefficient versus time lag are presented in the supporting information and show that the lags for the majority of coordinates have a single, clear peak. In Figure 1b, we saturate the color scale at 150 min which encapsulates most of the structure therein; in Figure 2b, we saturate the color scale at 240 min. Figure 2d shows the correlations with lower time lags saturated at 60 min to highlight the structure therein.

4.1. R1 and R2 Correlations

The shortest timescales observed in the dayside R1 and R2 correlations shown in Figure 1 are between 10 and 20 min. The dayside R1 correlations show this short timescale at their poleward edge, with timescales of ~60 min on the equatorward edge. We interpret this as a signature of the ECPC paradigm, since the current ovals will expand during southward B_z and thus j at high latitudes will react to southward B_z before j at lower latitudes. The dayside R2 correlation on the dusk side follows the same pattern, also consistent with the ECPC paradigm, with timescales approaching 90 min on the equatorward edge. However, the day/dawn R2 correlation is not as well described in this way: at 8 and 9 MLT the timescales are shorter on the equatorward edge, although the rest of the banding seems more consistent.

The X correlation in Figure 1 may be a signature of the expansion of the R1 and R2 current systems and therefore of the ECPC paradigm. As the polar cap expands with southward IMF, the initial coordinates of the polar cap will see a reduction of R1 current. This means that an expansion of the R1 current oval will manifest as a region of correlation in the opposite sense to the R1 correlation, like the X correlation. However, the timescales in these regions are ~50 min, which is much longer than the 10–20 min reported on the poleward edge of the R1 correlations: we explore alternative explanations for the X correlation in section 4.2.

On the nightside of Figure 1, the R1 and R2 correlations show longer timescales than on the dayside. The equatorward edge of the R1 correlation reacts with a timescale of 70–90 min, and the poleward edge reacts with a timescale of 120–150 min. This is again consistent with the ECPC paradigm, which would suggest that the longest timescales on the nightside are the currents flowing at the point where the polar cap has contracted at the end of a period of nightside reconnection (e.g., a substorm). The nightside R2 correlation on the dawn side follows the same pattern, with timescales between 30 min on the equatorward edge and 100 min on the poleward edge. The night/dusk R2 correlation, similar to the day/dawn correlation, does not seem as well described by the ECPC paradigm, with shorter timescales on the poleward edge at 21–23 MLT.

The interpretation of the timescales within the context of the ECPC paradigm explains most of the observed lags in the R1 and R2 correlations. In the case of R1, which maps directly to the magnetopause on the dayside, we note that if we assume that the R1 current sheet is a thin current sheet which is moving with the boundary of the polar cap, the timescales here as a function of latitude are indicative of how R1 is moving equatorward and poleward due to magnetic reconnection in the ECPC paradigm. Since R1 maps directly

to the magnetopause, this does not necessarily imply that higher-frequency variability in the IMF does not affect the R1 current on smaller timescales. In the case of R2, the day/dawn and night/dusk correlations do not seem well described by the ECPC paradigm. The correlations at noon MLT poleward of 15° colatitude appear to react at very long timescales of 120 min, and timescales of 160–170 min poleward of 10° colatitude, which is also difficult to interpret within the ECPC paradigm. We will discuss these further in section 5.

4.2. Other Regions of Correlation

We now turn to the other regions of correlation on the dayside. The Y correlations (Figure 1) can be interpreted in terms of NBz currents, named for their occurrence during northward IMF (Iijima et al., 1984; Iijima & Shibaji, 1987; Zanetti et al., 1984). The NBz currents are of opposite polarity to the R1 and R2 currents, but since they are driven by positive B_z instead of negative B_z, any correlation with NBz will be of the same sense as the R1 correlations observed. The Y correlations show shorter lags (10–20 min) at the equatorward edge and longer lags (50–70 min) at their poleward edge, which can be interpreted as a signature of the ECPC paradigm if these correlations are associated with NBz currents. As northward B_z does not open magnetic flux, nightside reconnection during northward B_z will lead the polar cap to contract. This means that, during northward B_z, j at lower latitudes will react to the solar wind driver before j at higher latitudes, giving this signature.

Alternatively, cusp currents may be responsible for the Y, A, and B correlations. Saunders (1989) argued that cusp currents were caused by field lines shortening over the dayside magnetopause, leading to field tension imparting an east/west component of motion, and further argued that the cusp current was caused by the tilt in the magnetic field which resulted from the field lines changing direction to move antisunward across the polar cap. Figure 1 of Saunders (1989) reports the average cusp currents for the positive and negative B_y, both of which would be contained within our Figure 1a. When these average cusp currents are summed, the resulting pattern is very close to the Y correlation in our Figure 1a. Taking the difference of the average cusp currents gives a signature very close to the A and B correlations in our Figure 2a, which is consistent with the prevailing negative B_y observed during March 2010. The timescales in our Figure 2d are 15–30 min, indicating a near-instantaneous effect of the B_y component of the IMF on the dayside Birkeland currents.

The description of Saunders (1989) does not appear to be inconsistent with the framework employed by Ohtani et al. (1995), who suggested that what they referred to as R0 currents were associated with the shear of antisunward convection flows as their velocities decrease toward the pole, on open field lines mapping into the plasma mantle. This would mean that the X correlation could be explained in a similar physical manner to the Y, A, and B correlations. The timescales for the X correlations are ∼50 min: interpreted in the ECPC paradigm, this would indicate that these currents are on field lines which have not yet fully convected over the polar cap and into the magnetotail, consistent with the explanation of Ohtani et al. (1995). This explanation is also consistent with observations of B_y made by Shore et al. (2019), who concluded that spatial features of their timescales were consistent with field lines convecting across the polar cap (albeit at timescales of 20–25 min).

Finally, we turn to the nightside to examine the C and D correlations in Figure 2. Following similar logic to the cusp currents (Saunders, 1989), when field lines twisted by B_y asymmetries reconnect there should be an associated field-aligned current which acts to untwist the field lines. This implies that the C and D correlations are associated with substorms occurring when the magnetotail has some B_y asymmetry. Figure 2b shows that the timescales for the C correlation are 90–150 min, whereas the D correlation appears to show generally slightly shorter timescales of 90–120 min. The shorter timelags appear to be on the poleward edge in the D correlation and the 21–23 sector in the C correlation. Longer timescales are observed in the 00–02 MLT and the 18–20 MLT sectors in both the C and D correlations; we will discuss the timescales in the context of the literature in section 5.

5. Discussion

The correlations of B_z and j have the same large-scale structure as that previously seen in statistical patterns of Birkeland current. The overall structure in the R1 and R2 correlations in Figure 1a is reminiscent of the original patterns reported by Iijima and Potemra (1978), but is even more similar to the clock angle relationships shown in Weimer (2001). Figure 1a's spiral structure in the positive correlations, with the negative correlations on either side, looks very similar to the pattern seen by Weimer (2001) for the case where both B_y and B_z were negative.

The correlations reported in Figures 1a and 2a are low compared with previous reports of the correlation of Birkeland current with IMF driving. Coxon et al. (2014a) reported that the correlation of the total R1 Birkeland current with dayside reconnection rate Φ_D was 0.60. Plotting the correlation of j with Φ_D in the polar cap for March 2010 (not shown) shows that the correlations are slightly higher than those in Figure 1a but the correlations reported in Coxon et al. (2014a) were ∼0.15 higher. By summing j across several local times, then noise which is uncorrelated in local time will cancel out, and the signal-to-noise of the summed j will therefore be higher than j in each coordinate. If that noise is uncorrelated with IMF, the reaction of the summed j to the IMF will also have a higher signal-to-noise ratio. This explains why the correlations seen in Figures 1a and 2a are lower than in previous studies which summed the currents spatially (e.g., Coxon et al., 2014a). We interpret the fidelity of our reported statistical patterns relative to those reported by Weimer (2001) as evidence that our technique yields physically meaningful results.

The timescales we report appear to be well explained by the ECPC paradigm, suggesting that the timescale of the poleward edge of the correlations in both B_y and B_z (10–20 min) corresponds to the timescale of the correlation as the polar cap begins to expand with dayside reconnection. Snekvik et al. (2017) found evidence for instantaneous response of Birkeland currents to driving by the IMF at noon and midnight MLT, which they interpreted in the context of Alfvén wave propagation. We find very low time lags at noon but not at midnight, which is in line with ECPC timescales. Interpreting our results within the ECPC paradigm suggests that the timescale of the equatorward edge on both the dayside and nightside is indicative of the point at which the polar cap reaches its largest point (60–90 min) and that the longest timescales on the nightside (120–150 min) are indicative of the end of a cycle of expansion and contraction. Currents at these timescales are not directly driven by the solar wind but are the integral of some process (or possibly, several processes) which occur at longer timescales and peak at the times shown in Figures 1b and 2b, which we refer to as an "integral response."

Our observed time lag of 10–20 min implies that the dayside currents in the unexpanded polar cap are directly driven by variability in the IMF, and is consistent with the timescales of B_y and ϵ on the dayside reported by Shore et al. (2019) of 15–25 min, and the dayside timescale of 20 min reported by Anderson et al. (2014). McPherron et al. (2018) reported the peak response of AMPERE-derived dayside currents to a universal coupling function as 40 min, which is longer than all three other studies mentioned above; the reasons for this are unclear. The ϵ timescales in Shore et al. (2019) are longer at the poleward edge of the correlation, rather than timescales increasing with distance equatorward as is seen here. From the difference in behavior between the B_z response in this study and in Shore et al. (2019), we infer that the OCB expands and contracts more than the apparent width of the R1/R2 current system but less than the apparent width of the electrojets as seen by SuperMAG.

The 60–90 min timescale that we infer to be indicative of the end of polar cap expansion (and by extension, the onset of nightside reconnection) is identical to the timescale found by Anderson et al. (2014) and is also consistent with timescales of ∼65 min reported by Shore et al. (2019) at a colatitude of 30°, who found similar behavior in MLT. McPherron et al. (2018) reported that the response of AMPERE-derived nightside currents to a universal coupling function peaked at 60 min, at the short end of our range. Our 120- to 150-min timescale, which we interpret as the end of a substorm cycle, is at the upper end of the timescale for the formation of the complete R1/R2 system given by Anderson et al. (2014) but is slightly shorter than the reported timescale for substorm periodicity reported by Freeman and Morley (2004), who found that the periodicity was 2.7–2.9 hr (162–174 min). However, our timescale of 150 min is only 12 min shorter than Freeman and Morley (2004)'s periodicity of 162 min, and the uncertainty in propagating the IMF from the L1 point to the bow shock, combined with the 10-min uncertainty in the sliding window for evaluating AMPERE data, may mean that when these uncertainties are considered these timescales are not inconsistent with one another.

As noted in section 4.1, the R2 correlations do not appear to be as easily described using the ECPC paradigm. The R2 correlations on the dayside/duskside and the nightside/dawnside are consistent with the ECPC paradigm, whereas those correlations in the other two quadrants are not. Analysis of the OMNI data for the month shows that the B_y component of the IMF was generally negative, and generally more negative than B_z. Comparison of Figure 2a with the analysis of Weimer (2001) shows that the correlation of j with B_y looks very similar to their result for purely negative B_y. As such, we interpret our observations in the context of

the ECPC paradigm, but with some rotation of the current systems introduced by a B_y asymmetry during the month, which explains the behavior of the R2 correlation.

In this paper, we have highlighted the manner in which the cusp currents can explain all of the non-R1 and R2 currents on the dayside, whereas the Y correlations can also be explained by the NBz current system and the X correlation can also be explained by the expansion of the R1 and R2 current ovals during periods of dayside driving. It is likely that each of these factors is contributing to the results presented herein, and we plan to employ case studies in the future to explore the relative contributions of each effect to our results.

The results shown in section 4.2 show that the timescales of B_y on the nightside are between 90 and 150 min, and that the timescales are smallest in the 21–23 MLT sector. This might imply substorms occur in the 21–23 sector preferentially and the timescales in the adjacent sectors are a result of the westward traveling surge and some similar eastward propagation (e.g., Tanaka et al., 2015). It is known that the B_y component of the IMF is a factor in the deviation of substorm onset MLT from the average substorm onset MLT of ~22 MLT (Wang et al., 2007), so it is perhaps also possible that these results imply more asymmetrical magnetotail lobe configurations result in delayed substorm onsets compared to those which occur at times when the magnetotail is less asymmetrical.

Previous work has disagreed on the relative timescales of B_y propagation into Earth's magnetotail. Some authors have argued that the timescales should be similar to those suggested by the convection speed of field lines as part of the Dungey cycle and ECPC paradigm (Browett et al., 2017; Fear & Milan, 2012) whereas others have employed an argument based around MHD waves to argue that the asymmetry propagates into the magnetotail on timescales of tens of minutes (Tenfjord et al., 2015, 2017, 2018). Since any change in the configuration of the Earth's magnetic field should be communicated to the ionosphere by Birkeland currents, we can use this analysis to test the timescales on which this occurs.

Our analysis supports the result of Browett et al. (2017), since we see time lags of the correlation in B_y between 90 and 120 min on the nightside (which Browett et al., 2017, inferred to be the timescale of B_y propagation during southward IMF), but we do not see much correlation at 180 min (inferred by Browett et al., 2017, as due to northward IMF). Since AMPERE currents are weaker for lower dayside driving and therefore weaker for northward IMF (Coxon, 2015), we infer from this that the signal from the southward IMF driving during our selected time is dominating over the signal from the northward IMF, especially on the nightside. Shore et al. (2019) reported B_y timescales were 20–25 min on the nightside, but the correlations they reported were entirely within 15° colatitude, and thus their nightside timescales are entirely spatially distinct from the nightside timescales we present in this paper. Shore et al. (2019) attributed the structure they observed in the correlations to field lines moving across the polar cap, which is the same logic employed by this paper and by Browett et al. (2017) in interpreting B_y timescales.

6. Conclusion

We lag the IMF B_y and B_z compared with the current density j reported by AMPERE in order to find the maximum correlation within a lag of 2 hr, and the time lag which yields that maximum correlation. We find that the maximum correlations are colocated with the constituent Birkeland current systems (Iijima & Potemra, 1978; Weimer, 2001), showing that they are influenced by B_y and B_z.

The time lags associated with the B_z correlations show that statistically, on the dayside, the poleward side of the R1 correlation is associated with a timescale of 10–20 min, before the equatorward edge of the R1 correlation at ~60 min. On the nightside, the equatorward edge of the R1 correlation has a timescale of 70–90 min and the poleward correlation has a timescale of 120–150 min. This is indicative of a process in which R1 currents form on the dayside colocated with the polar cap, expand with the polar cap, form on the nightside, and then contract with the polar cap as nightside reconnection occurs, and can therefore be easily interpreted in the ECPC paradigm (Cowley & Lockwood, 1992; Siscoe & Huang, 1985).

The time lags associated with the B_y correlations are evidence for models of IMF B_y propagation based around the convection of magnetic field lines (Browett et al., 2017; Cowley, 1981; Fear & Milan, 2012) which suggest timescales of propagation should be on the order of hours rather than the order of tens of minutes, as has previously been suggested (Tenfjord et al., 2018, 2015, 2017).

The timescales of the reaction of Birkeland currents to solar wind driving also indicate the timescales of the ionospheric response to solar wind driving, as it is the Birkeland currents which communicate stresses from

the magnetopause and magnetotail into the ionosphere. The technique we use to uncover these timescales, inspired by the SPIDER technique developed and applied to SuperMAG data by Shore et al. (2019), is novel in its application to AMPERE data, and makes relatively few assumptions about the system. We intend to exploit this technique with case studies in the future.

Acknowledgments
J.C.C. and R.C.F. were supported by Science and Technology Facilities Council (STFC) Ernest Rutherford grant ST/L002809/1 and Consolidated grant ST/R000719/1. R.M.S. and M.P.F. were supported by Natural Environment Research Council (NERC) grant NE/N01099X/1 and the SuperMAG EOF model was developed under NERC grant NE/J020796/1. R.C.F. was supported by STFC Ernest Rutherford Fellowship ST/K004298/2; S.D.B. was supported by STFC PhD studentship ST/M503794/1; A.W.S. was supported by a SEPnet PhD studentship; and D.K.W. was supported by NERC grant NE/N004051/1. J.C.C. and R.M.S. would like to thank the organizers and sponsors of the Russian-British Seminar of Young Scientists on "Dynamical plasma processes in the heliosphere: from the Sun to the Earth," which hosted discussions useful to this manuscript. The Iridium-derived AMPERE data used in this paper can be obtained from the AMPERE Science Center (at http://ampere.jhuapl.edu/). The OMNI data used in this paper can be obtained from NASA/GSFC's Space Physics Data Facility's CDAweb service (at http://cdaweb.gsfc.nasa.gov/). The authors would like to thank the AMPERE Science Center and NASA/GSFC for providing the data.

References

Anderson, B. J., Korth, H., Waters, C. L., Green, D. L., Merkin, V. G., Barnes, R. J., & Dyrud, L. P. (2014). Development of large-scale Birkeland currents determined from the active magnetosphere and planetary electrodynamics response experiment. *Geophysical Research Letters*, *41*, 3017–3025. https://doi.org/10.1002/2014GL059941

Anderson, B. J., Korth, H., Welling, D. T., Merkin, V. G., Wiltberger, M. J., Raeder, J., et al. (2017). Comparison of predictive estimates of high-latitude electrodynamics with observations of global-scale Birkeland currents. *Space Weather*, *15*, 352–373. https://doi.org/10.1002/2016SW001529

Anderson, B. J., Takahashi, K., & Toth, B. A. (2000). Sensing global Birkeland currents with Iridium engineering magnetometer data. *Geophysical Research Letters*, *27*(24), 4045–4048. https://doi.org/10.1029/2000GL000094

Birkeland, K. (1908). *The Norwegian Aurora Polaris Expedition 1902-1903* (Vol. 1). Christiania, Norway: H. Aschelhoug & Co.

Birkeland, K. (1913). *The Norwegian Aurora Polaris Expedition 1902-1903* (Vol. 2). Christiania, Norway: H. Aschelhoug & Co.

Browett, S. D., Fear, R. C., Grocott, A., & Milan, S. E. (2017). Timescales for the penetration of IMF B_y into the Earth's magnetotail. *Journal of Geophysical Research: Space Physics*, *122*, 579–593. https://doi.org/10.1002/2016JA023198

Clausen, L. B. N., Milan, S. E., Baker, J. B. H., Ruohoniemi, J. M., Glassmeier, K.-H., Coxon, J. C., & Anderson, B. J. (2013). On the influence of open magnetic flux on substorm intensity: Ground- and space-based observations. *Journal of Geophysical Research: Space Physics*, *118*, 2958–2969. https://doi.org/10.1002/jgra.50308

Cowley, S. W. H. (1981). Magnetospheric asymmetries associated with the y-component of the IMF. *Planetary and Space Science*, *29*(1), 79–96. https://doi.org/10.1016/0032-0633(81)90141-0

Cowley, S. W. H. (2000). Magnetosphere-ionosphere interactions: A tutorial review. In S.-I. Ohtani, R. Fujii, M. Hesse, & R. L. Lysak (Eds.), *Magnetospheric current systems* (Vol. 118, pp. 91–106), Geophysical Monograph Series. Washington, DC, USA: American Geophysical Union. http://www.agu.org/books/gm/v118/GM118p0091/GM118p0091.shtml

Cowley, S. W. H., & Lockwood, M. (1992). Excitation and decay of solar wind-driven flows in the magnetosphere-ionosphere system. *Annales Geophysicae*, *10*, 103–115.

Coxon, J. C. (2015). Birkeland currents and their role in the Dungey cycle (Ph.D. Thesis), University of Leicester, Leicester, UK.

Coxon, J. C., Milan, S. E., & Anderson, B. J. (2018). A review of Birkeland current research using AMPERE. In A. Keiling, O. Marghitu, & M. Wheatland (Eds.), *Electric currents in geospace and beyond* (pp. 257–278). Washington, DC: American Geophysical Union. https://doi.org/10.1002/9781119324522.ch16

Coxon, J. C., Milan, S. E., Carter, J. A., Clausen, L. B. N., Anderson, B. J., & Korth, H. (2016). Seasonal and diurnal variations in AMPERE observations of the Birkeland currents compared to modeled results. *Journal of Geophysical Research: Space Physics*, *121*, 4027–4040. https://doi.org/10.1002/2015JA022050

Coxon, J. C., Milan, S. E., Clausen, L. B. N., Anderson, B. J., & Korth, H. (2014a). The magnitudes of the regions 1 and 2 Birkeland currents observed by AMPERE and their role in solar wind-magnetosphere-ionosphere coupling. *Journal of Geophysical Research: Space Physics*, *119*, 9804–9815. https://doi.org/10.1002/2014JA020138

Coxon, J. C., Milan, S. E., Clausen, L. B. N., Anderson, B. J., & Korth, H. (2014b). A superposed epoch analysis of the regions 1 and 2 Birkeland currents observed by AMPERE during substorms. *Journal of Geophysical Research: Space Physics*, *119*, 9834–9846. https://doi.org/10.1002/2014JA020500

Coxon, J. C., Rae, I. J., Forsyth, C., Jackman, C. M., Fear, R. C., & Anderson, B. J. (2017). Birkeland currents during substorms: Statistical evidence for a region 2 intensification after onset and a local reduction in density before onset. *Journal of Geophysical Research: Space Physics*, *122*, 6455–6468. https://doi.org/10.1002/2017JA023967

Cummings, W. D., & Dessler, A. J. (1967). Field-aligned currents in the magnetosphere. *Journal of Geophysical Research*, *72*(3), 1007–1013. https://doi.org/10.1029/JZ072i003p01007

Dungey, J. W. (1961). Interplanetary magnetic field and the auroral zones. *Physics Review Letters*, *6*, 47–48.

Fear, R. C., & Milan, S. E. (2012). The IMF dependence of the local time of transpolar arcs: Implications for formation mechanism. *Journal of Geophysical Research*, *117*, A03213. https://doi.org/10.1029/2011JA017209

Freeman, M. P. (2003). A unified model of the response of ionospheric convection to changes in the interplanetary magnetic field. *Journal of Geophysical Research*, *108*(A1), SMP 14–1– SMP 14– 13. https://doi.org/10.1029/2002JA009385

Freeman, M. P., & Morley, S. K. (2004). A minimal substorm model that explains the observed statistical distribution of times between substorms. *Geophysical Research Letters*, *31*, L12807. https://doi.org/10.1029/2004GL019989

Greenwald, R. A., Baker, K. B., Ruohoniemi, J. M., Dudeney, J. R., Pinnock, M., Mattin, N., et al. (1990). Simultaneous conjugate observations of dynamic variations in high-latitude dayside convection due to changes in IMF B_y. *Journal of Geophysical Research*, *95*(A6), 8057–8072. https://doi.org/10.1029/JA095iA06p08057

Iijima, T., & Potemra, T. A. (1978). Large-scale characteristics of field-aligned currents associated with substorms. *Journal of Geophysical Research*, *83*(A2), 599–615. https://doi.org/10.1029/JA083iA02p00599

Iijima, T., Potemra, T. A., Zanetti, L. J., & Bythrow, P. F. (1984). Large-scale Birkeland currents in the dayside polar region during strongly northward IMF: A new Birkeland current system. *Journal of Geophysical Research*, *89*, 7441–7452. https://doi.org/10.1029/JA089iA09p07441

Iijima, T., & Shibaji, T. (1987). Global characteristics of northward IMF-associated (NBZ) field-aligned currents. *Journal of Geophysical Research*, *92*(A3), 2408–2424. https://doi.org/10.1029/JA092iA03p02408

Khurana, K. K., Walker, R. J., & Ogino, T. (1996). Magnetospheric convection in the presence of interplanetary magnetic field b_y: A conceptual model and simulations. *Journal of Geophysical Research*, *101*(A3), 4907–4916. https://doi.org/10.1029/95JA03673

King, J. H., & Papitashvili, N. E. (2014). One min and 5-min solar wind data sets at the Earth's bow shock nose. http://omniweb.gsfc.nasa.gov/html/HROdocum.html accessed on 16 October 2014.

McPherron, R. L., Anderson, B. J., & Chu, X. (2018). Relation of field-aligned currents measured by the network of Iridium spacecraft to solar wind and substorms. *Geophysical Research Letters*, *45*, 2151–2158. https://doi.org/10.1002/2017GL076741

Ohtani, S., Potemra, T. A., Newell, P. T., Zanetti, L. J., Iijima, T., Watanabe, M., et al. (1995). Simultaneous prenoon and postnoon observations of three field-aligned current systems from Viking and DMSP-F7. *Journal of Geophysical Research*, *100*(A1), 119–136. https://doi.org/10.1029/94JA02073

Pitkänen, T., Hamrin, M., Kullen, A., Maggiolo, R., Karlsson, T., Nilsson, H., & Norqvist, P. (2016). Response of magnetotail twisting to variations in IMF b_y: A THEMIS case study 1–2 January 2009. *Geophysical Research Letters*, *43*, 7822–7830. https://doi.org/10.1002/2016GL070068

Saunders, M. A. (1989). Origin of the cusp Birkeland currents. *Geophysical Research Letters*, *16*(2), 151–154. https://doi.org/10.1029/GL016i002p00151

Saunders, M. A., Freeman, M. P., Southwood, D. J., Cowley, S. W. H., Lockwood, M., Samson, J. C., et al. (1992). Dayside ionospheric convection changes in response to long-period interplanetary magnetic field oscillations: Determination of the ionospheric phase velocity. *Journal of Geophysical Research*, *97*(A12), 19,373–19,380. https://doi.org/10.1029/92JA01383

Shore, R. M., Freeman, M. P., Coxon, J. C., Thomas, E. G., Gjerloev, J. W., & Olsen, N. (2019). Spatial variation in the responses of the surface external and induced magnetic field to the solar wind. *Journal of Geophysical Research: Space Physics*, *124*. https://doi.org/10.1029/2019JA026543

Siscoe, G. L., & Huang, T. S. (1985). Polar cap inflation and deflation. *Journal of Geophysical Research*, *90*(A1), 543–547. https://doi.org/10.1029/JA090iA01p00543

Snekvik, K., Østgaard, N., Tenfjord, P., Reistad, J. P., Laundal, K. M., Milan, S. E., & Haaland, S. E. (2017). Dayside and nightside magnetic field responses at 780 km altitude to dayside reconnection. *Journal of Geophysical Research: Space Physics*, *122*, 1670–1689. https://doi.org/10.1002/2016JA023177

Southwood, D. J., & Hughes, W. J. (1983). Theory of hydromagnetic waves in the magnetosphere. *Space Science Reviews*, *35*(4), 301–366. https://doi.org/10.1007/BF00169231

Tanaka, Y., Ogawa, Y., Kadokura, A., Partamies, N., Whiter, D., Enell, C.-F., et al. (2015). Eastward-expanding auroral surges observed in the post-midnight sector during a multiple-onset substorm. *Earth, Planets and Space*, *67*(1), 182. https://doi.org/10.1186/s40623-015-0350-8

Tenfjord, P., Østgaard, N., Haaland, S., Snekvik, K., Laundal, K. M., Reistad, J. P., et al. (2018). How the IMF b_y induces a local b_y component during northward IMF b_z and characteristic timescales. *Journal of Geophysical Research: Space Physics*, *123*, 3333–3348. https://doi.org/10.1002/2018JA025186

Tenfjord, P., Østgaard, N., Snekvik, K., Laundal, K. M., Reistad, J. P., Haaland, S., & Milan, S. E. (2015). How the IMF B_Y induces a B_Y component in the closed magnetosphere and how it leads to asymmetric currents and convection patterns in the two hemispheres. *Journal of Geophysical Research: Space Physics*, *120*, 9368–9384. https://doi.org/10.1002/2015JA021579

Tenfjord, P., Østgaard, N., Strangeway, R., Haaland, S., Snekvik, K., Laundal, K. M., et al. (2017). Magnetospheric response and reconfiguration times following IMF b_y reversals. *Journal of Geophysical Research: Space Physics*, *122*, 417–431. https://doi.org/10.1002/2016JA023018

Wang, H., Lühr, H., Ma, S. Y., & Frey, H. U. (2007). Interhemispheric comparison of average substorm onset locations: Evidence for deviation from conjugacy. *Annales Geophysicae*, *25*(4), 989–999. https://doi.org/10.5194/angeo-25-989-2007

Waters, C. L., Anderson, B. J., & Liou, K. (2001). Estimation of global field-aligned currents using the Iridium system magnetometer data. *Geophysical Research Letters*, *28*(11), 2165–2168. https://doi.org/10.1029/2000GL012725

Weimer, D. R. (2001). Maps of ionospheric field-aligned currents as a function of the interplanetary magnetic field derived from Dynamics Explorer 2 data. *Journal of Geophysical Research*, *106*(A7), 12,889–12,902. https://doi.org/10.1029/2000JA000295

Zanetti, L. J., Potemra, T. A., Iijima, T., Baumjohann, W., & Bythrow, P. F. (1984). Ionospheric and Birkeland current distributions for northward interplanetary magnetic field: Inferred polar convection. *Journal of Geophysical Research*, *89*(A9), 7453–7458. https://doi.org/10.1029/JA089iA09p07453

Zmuda, A. J., Martin, J. H., & Heuring, F. T. (1966). Transverse magnetic disturbances at 1100 kilometers in the auroral region. *Journal of Geophysical Research*, *71*, 5033–5045.